

See discussions, stats, and author profiles for this publication at: <https://www.researchgate.net/publication/278089221>

Conformational Analysis of Gly Ala NHMe in D₂O and DMSO Solutions: A Two-Dimensional Infrared Spectroscopy Study

ARTICLE in THE JOURNAL OF PHYSICAL CHEMISTRY B · NOVEMBER 2013

Impact Factor: 3.3 · DOI: 10.1021/jp406139t

READS

24

10 AUTHORS, INCLUDING:



Elena Ragnoni

Universität Siegen

6 PUBLICATIONS 17 CITATIONS

[SEE PROFILE](#)



Chiara Cappelli

Scuola Normale Superiore di Pisa

117 PUBLICATIONS 1,866 CITATIONS

[SEE PROFILE](#)



Benedetta Mennucci

Università di Pisa

250 PUBLICATIONS 24,304 CITATIONS

[SEE PROFILE](#)



Paolo Foggi

Università degli Studi di Perugia

119 PUBLICATIONS 1,642 CITATIONS

[SEE PROFILE](#)

Conformational Analysis of Gly–Ala–NHMe in D₂O and DMSO Solutions: A Two-Dimensional Infrared Spectroscopy Study

Marco Candelaresi,[†] Elena Ragnoni,[‡] Chiara Cappelli,^{§,⊥} Alessandro Corozzi,^{||} Manuela Lima,^{‡,■} Susanna Monti,[▲] Benedetta Mennucci,[⊥] Francesca Nuti,^{●,¶} Anna Maria Papini,^{●,¶,#} and Paolo Foggi*,^{‡,■,▼}

[†]Heriot-Watt University, Edinburgh Campus, Edinburgh, Scotland EH14 4AS

[‡]LENS, Polo Scientifico Universitario, Via Nello Carrara 1, 50019 Sesto F.no (FI), Italy

[§]Scuola Normale Superiore, Piazza dei Cavalieri 7, 56126 Pisa, Italy

[⊥]Dipartimento di Chimica e Chimica Industriale, Università di Pisa, Via Risorgimento 35, 56126 Pisa, Italy

^{||}Technical University of Denmark—Department of Chemistry, Kemitorvet, Kongens Lyngby, DK 2800, Denmark

[■]INO-CNR, Polo Scientifico Universitario, Via Nello Carrara 1, 50019 Sesto F.no (FI), Italy

[▲]CNR ICCOM, Area della Ricerca, Via G. Moruzzi 1, 56124 Pisa, Italy

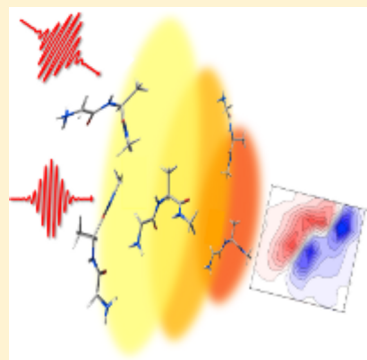
[●]French-Italian Laboratory of Peptide & Protein Chemistry & Biology (www.peptlab.eu); [¶]Dipartimento di Chimica, Università di Firenze, Polo Scientifico Universitario, Via delle Lastruccia 13, 50019 Sesto F.no (FI), Italy

[#]Laboratoire SOSCO EA 4505, Université de Cergy-Pontoise, 5 Mail Gay Lussac, 95031 Cergy-Pontoise, France

[▼]Dipartimento di Chimica, Università di Perugia, Via Elce di Sotto 8, 06100 Perugia, Italy

Supporting Information

ABSTRACT: A relevant number of experiments on short peptides has been performed in recent years. One of the major problems rises from the simultaneous presence of slightly different conformers at equilibrium in solution. In the present paper, the conformational characteristics of the Gly–L-Ala–Methyl amide dipeptide in D₂O and DMSO solutions are investigated by nonlinear IR spectroscopy. The pump–probe scheme with ultrashort mid-infrared pulses, in the Amide I region, is used to determine the mutual orientation of the two C=O bonds and the dynamics due to solute–solvent interactions. The coupling between Amide I modes is evaluated from both linear and 2D spectra. The interconversion between the different conformations occurs on time scales longer than the vibrational lifetime, and the spectral diffusion observed in 2D spectra is attributed to the solvent dynamics. Quantum mechanical calculations and molecular dynamics simulations are performed to identify the most stable geometries. By comparing the experimental and the theoretical data, we establish the prevalence of β -like polar conformers in both water and DMSO solvents.



1. INTRODUCTION

Infrared spectroscopy is used qualitatively and semiquantitatively to detect changes in protein backbone conformations even in the presence of inhomogeneous broadening and spectral congestion. Specific spectral features can be correlated, for example, to the amount of α -helices, β -sheets, and random coils present in a protein.¹

The Amide I mode in the 6 μm region, which mainly involves the internal coordinate C=O stretching, is very sensitive to the protein secondary structure, as its central frequency varies with the surrounding changes.² This vibrational mode has a large transition dipole moment making it easily observable in the steady-state IR spectra, in a region generally free from interferences due to other spectral components. This mode is used in linear IR spectroscopy as a marker of the peptide chain conformations.

The development of stable femtosecond sources³ delivering tunable pulses in the mid-infrared region has allowed the growth of new nonlinear spectroscopic tools capable of providing additional information to those obtained by steady-state IR absorption.^{4–9} Some of them allow for the extraction of homogeneous line width from the inhomogeneous one and open up the possibility of achieving precise spectroscopic details in “in vivo” conditions, that is, at temperatures and concentrations where relaxation processes and the distribution of the conformations obscure many spectral details. Recent studies have shown that structural and dynamical properties of biomolecules at room temperature in solution can be achieved by two-dimensional infrared spectroscopy.^{5–14}

Received: June 21, 2013

Published: October 28, 2013

Two-dimensional infrared spectroscopy (2D-IR) is one of the IR nonlinear techniques able to disentangle the homogeneous contribution from inhomogeneous bands, this separation being not possible with classical stationary IR spectroscopy. The 2D-IR technique undergoes similar rules of 2D-NMR^{7–9,14–16} spectroscopy, but it can achieve a time resolution 5 orders of magnitude higher (i.e., in the picosecond or even in the subpicosecond regime). On this time scale it is possible to “freeze” short-living high-energy conformers of small molecules, which cannot be discriminated through NMR spectroscopy.

Combining the results of 2D-IR experiments with those obtained by ab initio calculations and MD simulations,¹⁷ one can estimate the dihedral angles θ and Ψ of each peptide bond and determine secondary structure motifs such as α -helices and β -sheets. Recent results obtained in systems of diverse complexity are very promising.^{18–20}

Relatively simple molecules like short peptides are very interesting benchmarks for testing computational results, comparing them to experimental findings, and defining strong protocols which could be used to investigate and predict the structure of more complex systems. In order to accomplish these goals, it is convenient to start from dipeptides, tripeptides, and short polypeptides^{5,10,21–27} and then extend the investigation to more complex systems, such as phospholipids membranes,²⁸ systems with α -helices²⁹ and β -sheets,³⁰ proteins, and DNA oligonucleotides.^{19,20} Simple peptides have been used not only as model systems but also as leading compounds for biomedical applications. Indeed, they actively participate in different kinds of processes as inhibitors,³¹ selective receptors, and enzyme regulators,^{32–34} where specific conformations play an important role in their activity.

The main goal of the present study is to investigate the influence of the solvent in stabilizing specific conformations of the Glycine-L-Alanine-Methyl amide (GANHMe) dipeptide. In this molecule, two peptide bonds are presents.^{14,27} The conformation of the molecule is essentially defined by the backbone dihedral angles as shown in Figure 1.

2. EXPERIMENTAL AND THEORETICAL METHODS

2.1. Sample Synthesis.

GANHMe and GA*NHMe (^{13}C -labeled at the C=O of the L-alanine moiety) were synthesized

in our laboratory, by using differently labeled amino acids as building blocks in an optimized peptide synthesis strategy, summarized in the following steps.

STEP 1: Synthesis of L-Alanine N-methylamide Hydrochloride [H-Ala-NHMe·HCl]. A solution of methylamine hydrochloride (1 eq, 1.75 mmol, 118 mg) and Et₃N (1 eq, 246 μL) in DMF (3 mL) was added to a solution of Boc-Ala-OSu (1 eq, 1.75 mmol, 500 mg) in DMF (5 mL). After stirring overnight at rt, the reaction mixture was filtered. Then, excess reagent and solvent were removed under vacuum. The crude product was extracted with DCM (2 \times 10 mL) and washed with H₂O (2 \times 3 mL). The combined organic solutions were dried with Na₂SO₄ and concentrated to give Boc-Ala-NHMe (R_f [DCM/MeOH, 20:1; Cl₂/tolidine] = 0.66). To a solution of Boc-Ala-NHMe in anhydrous CH₂Cl₂ (12 mL), concd HCl (5 mL) was added, and the reaction mixture was stirred for 1 h at rt. Then, excess reagent and the solvent were removed under vacuum. The N-methyl amide 1 was dissolved in H₂O and lyophilized (85% yield). Analytical and spectral data are in agreement with literature.³⁵

STEP 2: Synthesis of Glycyl-L-Alanine N-methylamide Hydrochloride [H-Gly-Ala-NHMe·HCl]. To a solution of 1 (1 eq, 1.48 mmol, 205 mg) and Et₃N (1 eq, 206 mL) in DMF (3 mL), a solution of Boc-Gly-OSu (1 eq, 1.48 mmol, 402 mg) in DMF (5 mL) was added. After stirring overnight at rt, the reaction mixture was filtered, and then the solvent was removed under vacuum. The crude product was extracted with DCM (2 \times 10 mL) and washed with H₂O (2 \times 3 mL) (R_f [DCM/MeOH, 15:1; Cl₂/Tolidine] = 0.56). The combined organic solutions were dried over Na₂SO₄ and concentrated to give Boc-Gly-Ala-NHMe. The protected dipeptide was treated with concd HCl as described for the compound 1. The dipeptide 2 was purified by semipreparative RP-HPLC (model 600, Waters) on a Jupiter C18 or C8 column (10 mm, 25 cm, 10 mm) at 4 mL/min. [Method: 0–30% B in 20 min. The solvent systems used were A (0.1% TFA in H₂O) and B (0.1% TFA in CH₃CN)]. Fractions were checked by analytical UPLC-ESIMS and then lyophilized. The pure product 2 (1.04 mmol, 202 mg, yield 70%) was dissolved in an acid solution DCl/D₂O three times. Analytical and spectral data are in agreement with the literature.³⁶ HPLC, Rt (min): 4.879, method 0–30% B in 20 min. ESI-MS *m/z*: [M+H]⁺ calcd 159.19; found, 160.17.

All samples were lyophilized from D₂O and DCl solutions to deuterate the NH groups and to remove TFA residues.

2.2. Laser Apparatus and Sample Handling. The laser setup consists of a Ti:Sapphire oscillator and amplifier system (Legend Elite, Coherent). A portion of the output is a 1 kHz train of 700 μJ pulses at 800 nm with temporal width \leq 50 fs. Its output is split into equal parts to pump two traveling-wave optical parametric amplifiers (OPA). The pump radiation in this experiment is generated by a TOPAS (Light Conversion Ltd.). The probe and reference beams are produced by a homemade OPA.³⁷ It is possible therefore to tune independently the pump and the probe wavelengths in order to achieve, if necessary, two-color 2D-IR spectra.

Mid-infrared (MIR) pulses, around 6 μm , are obtained by difference-frequency generation of the signal and idler pulses in an AgGaS₂ crystal. The MIR output has a spectral width of \geq 200 cm^{-1} and energy on the order of 1 $\mu\text{J}/\text{pulse}$. The pump beam passes through a half-wave plate, which allows the polarization to be set parallel or perpendicular to that of the probe and then through a variable delay line. The probe and

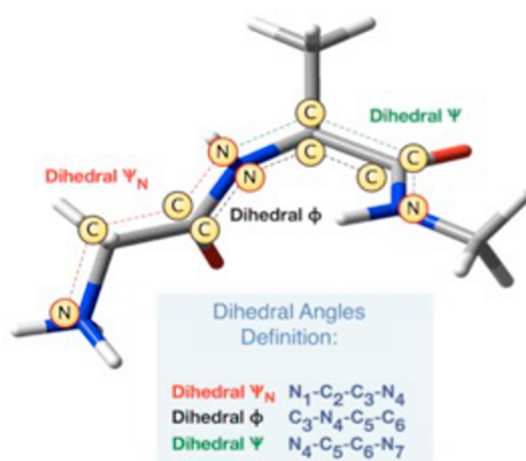


Figure 1. Glycine-L-Alanine-Methyl amide (GANHMe) dipeptide: definition of the three torsional angles ψ_N , ϕ , and ψ .

reference beams are the two reflections from the faces of a wedged CaF_2 plate. Pump, probe, and reference beams are focused into the sample by means of a parabolic mirror. The probe and reference beams are imaged into a flat-field monochromator (TRIAX 180, HORIBA Jobin Yvon) equipped with a double 32-channel array of Mercury Cadmium Telluride (MCT) detectors (InfraRed Associates, Inc.) kept at low temperature by a liquid nitrogen reservoir. The pump beam is chopped at half the laser repetition rate, and the signal is acquired as the difference between sequential pump-on/pump-off measurements. In this way, effects due to long-term laser drift are eliminated. A homemade front-end³⁸ and an acquisition software transfer calculate the ΔOD signals as the average of several separate acquisitions and as a function of the delay between pump and probe pulses.

By averaging over 10 000 pulses, it is possible to achieve a noise/signal contrast ratio, which allows the observation of signals well below the $10 \mu\text{OD}$ level. Broadband excitation spectra are recorded with a time resolution of ≈ 200 fs.

In order to accomplish narrowband pump experiments, the pump pulse passes through an infrared Fabry–Perot filter consisting of two reflectors ($R \approx 95\%$) separated by a distance, which is regulated by a feedback-controlled piezoelectric mount. In this configuration, the pump pulse has a bandwidth of $\approx 15 \text{ cm}^{-1}$ and a duration of ~ 800 fs. In order to produce 2D-IR spectra, transient spectra are recorded as a function of pump frequency for fixed delays.

The experiments were carried out on ~ 0.01 M solutions of GANHMe in D_2O and DMSO. The samples were kept in a homemade cell equipped with 2 mm thick CaF_2 windows separated by 50 or 75 μm Teflon spacers.

2.3. Quantum Mechanical Calculations. The structures of GANHMe stable conformations were optimized at the DFT level by using the B3LYP hybrid functional and the 6-311+ +G(d,p) basis set both in water and DMSO solution. Solvent effects were described by exploiting a continuum approach by means of the integral equation formalism (IEF)^{39,40} version of PCM, as implemented in the Gaussian03 code (G03).^{41,42} The PCM has been amply proven to reliably describe the structure and vibrational spectroscopic properties of peptide prototypes in solution.^{43–47}

The molecular cavity surrounding the solute molecule was built by interlocking spheres centered on carbon, oxygen, and nitrogen atoms. The radius of each sphere was obtained by scaling the corresponding van der Waals radius by 1.2 for water and 1.4 for DMSO. Free energies were calculated by including zero-point and thermal contributions. IR frequencies were obtained in the harmonic approximation.

2.4. Molecular Dynamic Simulations. Both initial set up and dynamic runs were performed with the AMBER9 program⁴⁸ using an explicit representation of solvent molecules and the ff03 all-atom force field,^{49,50} which is known to compensate for the propensity of the ff99 force field to oversample the right/handed helix conformation.^{51,52} Water was described by the TIP3P model,⁵³ whereas DMSO was represented by the flexible model developed by Kollman and co-workers.⁵⁴ All MD simulations were performed in the NpT ensemble at constant pressure (1 bar). Such a pressure was maintained using the Berendsen's barostat⁵⁵ and temperature relaxation time equal to 1 ps. The simulations were also performed at constant temperature ($T = 300$ K) maintained by coupling the system to a thermal bath with the Andersen's algorithm^{56,57} and pressure relaxation time equal to 1 ps. All

Lennard–Jones interactions were cut off at 12 Å and a Particle Mesh Ewald (PME) correction to long-range electrostatic interactions was applied. The integration step was set to 1 fs. GANHMe was surrounded by a periodic parallelepiped box of solvent molecules measuring $30 \times 30 \times 30$ and $44 \times 43 \times 45$ Å³ in the case of water and DMSO, respectively. A charge-balancing Cl^- counterion was added to neutralize the charge on the peptide surface. The system consisted of a peptide molecule, a Cl^- counterion, and 894 TIP3P waters in the simulations in aqueous solution. In the simulations of DMSO solution, it contained the peptide, the Cl^- counterion, and 711 molecules of DMSO. All the MD runs were set up using the same protocol. First, the system was subjected to 1000 steps of minimization to remove close van der Waals contacts and to allow the formation of hydrogen bonds between solvent molecules and the peptide. Then, it was heated up to 300 K gradually over 30 ps of constant volume dynamics while keeping fixed the solute coordinates. Equilibration at $T = 300$ K continued for 15 ps, in the NVT ensemble, to remove unphysical voids, and was followed by a 50-ps equilibration run at constant pressure. Starting from the equilibrated system, MD trajectories were recorded for a maximum of 6 ns and the data sampled every 0.5 ps. The last 5 ns were used for the analysis (10 000 configurations). In order to study the influence of water molecules on the structure and dynamics of GANHMe, restraints on peptide geometry were removed and a simulation, starting from the last solvent configuration sampled during the restrained dynamics, was conducted for 5 ns.

3. RESULTS AND DISCUSSION

3.1. EXPERIMENTAL RESULTS. 3.1.1. Linear Spectra.

Figure 2 shows the FTIR absorption spectra of GANHMe and

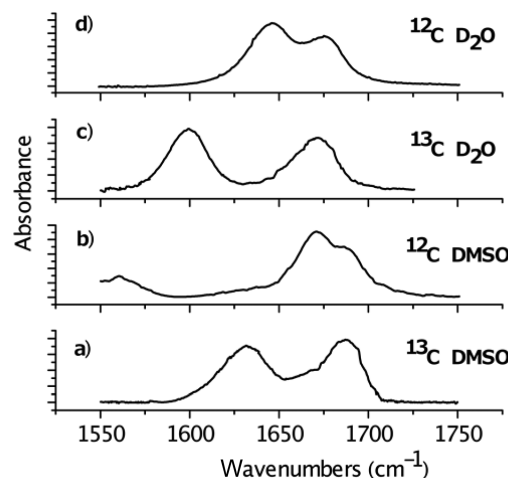


Figure 2. FT-IR spectra in D_2O and DMSO of GANHMe and GA*NHMe recorded in the 6 μm region. The band at higher frequencies is assigned to the Amide I mode of the Glycine residue and that at lower frequencies to the Amide I mode of the L-Alanine residue. The latter shifts along with the isotopic substitution. In spectrum (b), the Amide II band is partially visible around 1560 cm^{-1} .

GA*NHMe in DMSO and D_2O around 6 μm . In this region, the Amide I mode associated mainly to the $\text{C}=\text{O}$ stretching is visible; the Glycine residue gives the signal at higher frequencies, while at lower frequencies the L-Alanine CO shifts in accordance with the ^{13}C isotopic substitution. For GANHMe in DMSO, the Amide II at 1560 cm^{-1} is present too. Since

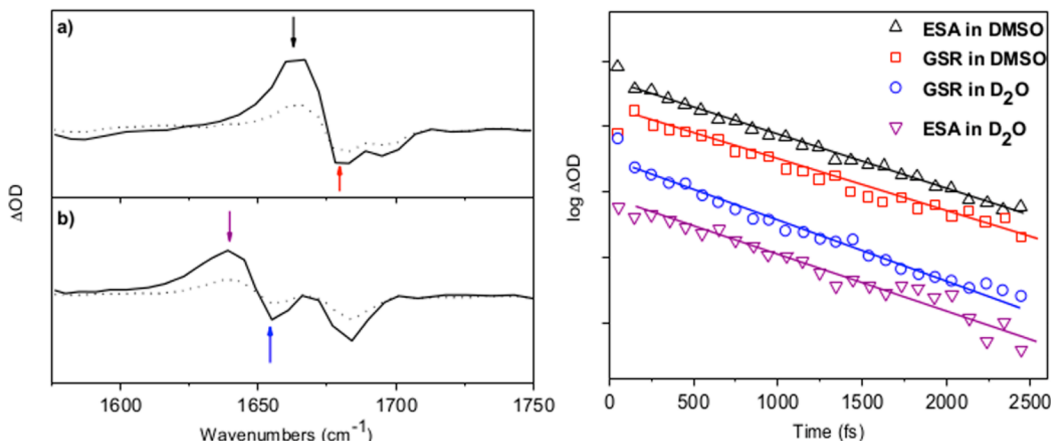


Figure 3. On the left, pump–probe spectra recorded at 0 ps (solid line) and 1 ps (dotted line) in broadband configuration for (a) GANHMe in DMSO and (b) in D₂O. The higher intensity of spectra in DMSO is due to the higher sample solubility. The arrows indicate the excited-state absorption and the bleaching-stimulated emission peaks where kinetics are characterized (log plots on the right). The sign of the GSR signals were changed to compare them with those of ESA. An averaged Amide I vibration lifetime of 1.2 ± 0.2 ps is extracted.

Amide II and III are usually assigned to the in-phase and out-of-phase C–N stretching and CNH bending mode combination, in D₂O the coupling is lost upon deuteration, and both transitions shift below 1500 cm⁻¹, out of the present spectral window.

The two Amides I in DMSO are not well-resolved, showing a main peak and a shoulder at higher frequencies. After a deconvolution process, the maxima of the two bands are located at 1689 ± 1 and 1671 ± 1 cm⁻¹. GANHMe in D₂O shows clearly two bands with maxima at 1674.7 ± 0.5 and 1646.3 ± 0.5 cm⁻¹, respectively. Isotopic substitution (GA*NHMe) provides well-separated bands in both DMSO and D₂O. The FTIR spectrum in D₂O exhibits two bands with maxima at 1671.8 ± 0.5 and 1599.3 ± 0.5 cm⁻¹, while in DMSO the maxima are at 1686.3 ± 0.5 and 1631.7 ± 0.5 cm⁻¹.

A first survey of the linear IR spectra brings the following observations. The separation between Amide I modes is more than 10 cm⁻¹. This cannot be ascribed only to the coupling effect between the two modes. As observed previously, the Amide I mode near a protonated N terminal, in the present case that of Glycine, generally occurs at higher frequencies.^{10,58,59} In D₂O, both bands shift to lower frequencies, the one ascribed to L-Alanine being more shifted than that of Glycine. As a result, the separation increases around 30 cm⁻¹. This effect must be due to a different average number of hydrogen bonds formed by the two C=O moieties. The additional effect of ¹³C C=O labeling is to further red shift the L-Alanine Amide I about 30 cm⁻¹. Assuming the frequency values are due to two close but different coupled oscillators, neglecting any effect of isotope substitution on the coupling mechanism and following the procedure described in ref 23, it is possible to calculate the coupling constants (see Supporting Information). These result to be 7 ± 3 cm⁻¹ in DMSO and 10 ± 2 cm⁻¹ in D₂O. These values are comparable to previously reported coupling constants.

3.1.2. Time-Resolved Experiments. Figure 3 shows the spectral evolution obtained in broad pump experiments on GANHMe in DMSO and D₂O.

The vertical arrows in the spectra indicate where the signal has been characterized in the time domain. The dynamics measured at the maximum of the positive ΔOD peak should provide the evolution of the excited-state absorption (ESA),

while that measured at the negative one, that of the ground-state recovery (GSR). Since ESA and GSR bands of the two coupled C=O modes are spectrally overlapped, an averaged value of vibrational lifetime is extracted from the log plot of kinetics. All the reported decay profiles are fitted by the same exponential: the vibrational lifetime of Amide I mode in GANHMe is 1.2 ± 0.2 ps, in agreement with values reported for similar systems.¹³

3.1.3. Pump–Probe 2D Spectra. The 2D spectra of GANHMe in DMSO and D₂O, acquired with the pump polarized parallel and perpendicular to the probe and at different delays, are shown in Figures 4 and 5.

In 2D spectra, if two vibrational modes are coupled, the selective excitation of a single mode generates a signal at the frequency of the coupled one. As a result, a cross peak is observed in the off-diagonal region.^{5,7,14} Along the principal

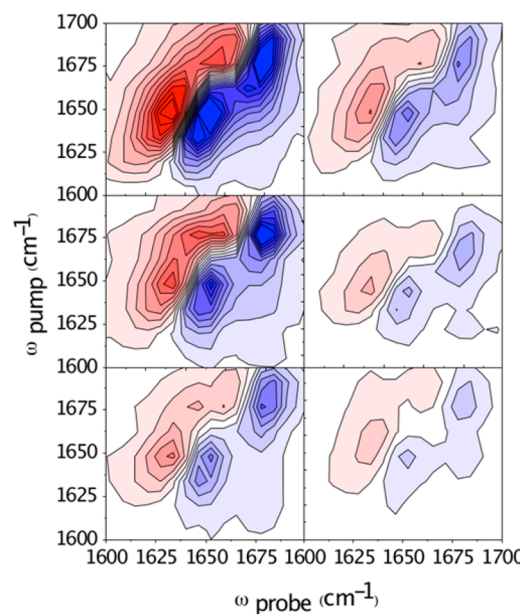


Figure 4. Two-dimensional-IR spectrum of GANHMe in D₂O recorded with parallel and perpendicular polarization on the left and right, respectively. From top to bottom: 0.5, 1.0, and 1.5 ps delays.

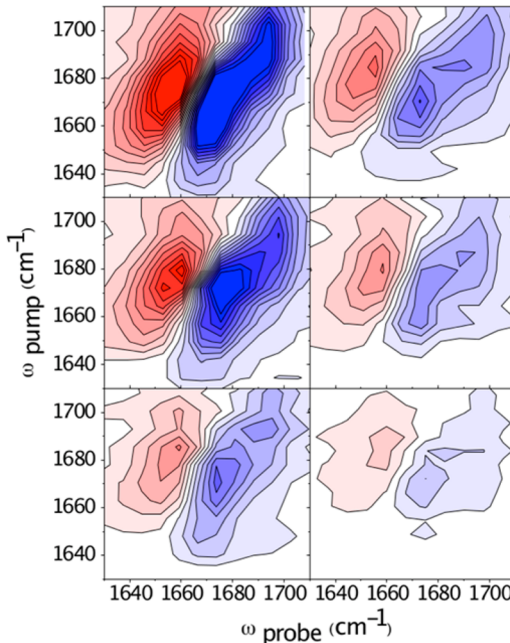


Figure 5. Two-dimensional-IR spectrum of GANHMe in DMSO recorded with parallel and perpendicular polarization on the left and right, respectively. From top to bottom: 0.5, 1.0, and 1.5 ps delays.

diagonal of 2D spectra, one observes the bleaching and the stimulated emission providing negative ΔOD signals. At lower probe frequencies, the $n = 1$ excited-state absorptions appear as positive ΔOD signals. The splitting is due to the anharmonicity, which in the present case is $\approx 18 \text{ cm}^{-1}$, a value close to that measured in NMA¹³ and in other peptides.^{5,10} The peak width measured at $t = 0 \text{ ps}$ along the antidiagonal is the homogeneous width^{7,14} convoluted with the pump width. The antidiagonal line width generally increases for positive delays due to “spectral diffusion”.¹⁴ The presence of positive absorption and negative bleaching signals gives rise along the 2D plot diagonal to a “zero intensity” line. At positive delay times, the latter tilts toward the vertical position as a consequence of the spectral diffusion.¹⁴ If it occurs on a slower time scale than the vibrational relaxation process, 2D features remain elongated, as observed in DMSO (see Figure 5). In the D_2O solutions, the spectral diffusion occurs on a time scale comparable to that of the vibrational relaxation, and an evolution toward the vertical line is clearly observed. Such a process is less pronounced for the L-Alanine Amide I than for the Glycine Amide I, which is almost vertical already at 0.5 ps (see Figure 4), implying a faster solvent dynamics around the Glycine C=O moiety. The elliptical contours with the long axis along the diagonal mark the presence of several solvent–solute conformers. A supermolecule approach⁴¹ is therefore needed to describe the inhomogeneity of the system. Its evolution describes the observed spectral diffusion (see section 3.2).

In both solvents, diagonal peaks have an asymmetric shape due to the presence of cross peaks. The small separation in the frequency of the Amide I bands in comparison to their inhomogeneous line width prevents any clear evaluation of cross peak intensity and position. This problem is overpassed in 2D spectra of GA*NHMe. Figure 6 shows the clear presence of cross peaks in both 2D spectra recorded in parallel and perpendicular polarization at 0.5 ps delay time.

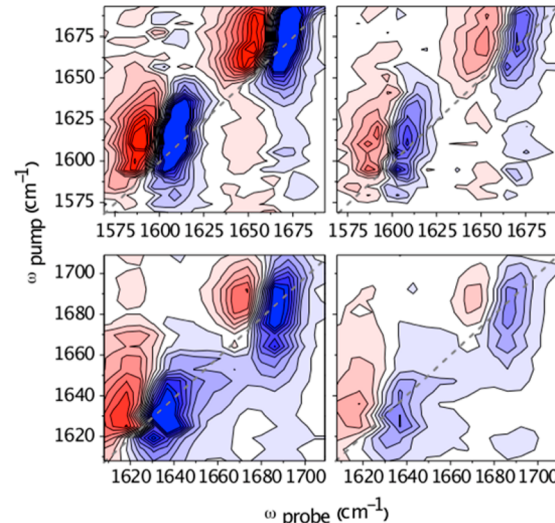


Figure 6. Two-dimensional-IR spectrum of GA*NHMe in D_2O (top) and DMSO (bottom) recorded in parallel and perpendicular polarization (on the left and right, respectively) at 0.5 ps.

By applying the vibrational exciton model^{7,23,60} on pump/probe spectra obtained by cutting the 2D contours at specific pump frequencies (see Supporting Information), a coupling constant of $10 \pm 4 \text{ cm}^{-1}$ is calculated for DMSO and $15 \pm 4 \text{ cm}^{-1}$ for D_2O . These values agree well with the coupling constants evaluated from the linear spectra (see previous section).

In order to validate the most stable calculated geometries, the angle θ_{12} between the transition dipole moments can be extracted from the off-diagonal anisotropy:

$$a_{12} = \frac{I_{\parallel} - I_{\perp}}{I_{\parallel} + 2I_{\perp}} \quad (1)$$

where I_{\parallel} is the intensity of the cross peak when the polarizations of pump and probe are parallel, and I_{\perp} is the intensity when the polarizations are perpendicular. The angle θ_{12} is then calculated according to the following equation obtained within the pump–probe scheme:^{14,60}

$$a_{12} = \frac{1}{5}(3\cos^2 \theta_{12} - 1) \quad (2)$$

By applying eq 2, the obtained values are $\theta_{12} = 60^\circ \pm 8^\circ$ in D_2O and $40^\circ \pm 10^\circ$ in DMSO (or their supplementary angles). This value of θ_{12} represents the result of an average over different conformations, which are present in solution at room temperature. In order to discriminate among conformers, QM calculations and MD simulations have been performed. A population-weighted value of θ_{12} is finally compared with the experimental one (see next section).

3.2. THEORETICAL RESULTS. 3.2.1. Conformational Study of GANHMe in Water. Comprehensive conformational analysis for analogous peptides has been carried out by other authors.⁶¹ With respect to their studies, we have chosen the most similar system⁶² and explored those backbone arrangements, which were reported as minimum energy conformers in solution. The minima found on the Ramachandran map of the L-Alanine dipeptide in water were used to rebuild GANHMe representative conformations (Figure 7).

As reported in ref 62, the most stable conformers in vacuum, in the gas phase, and in nonpolar solvents are the C5

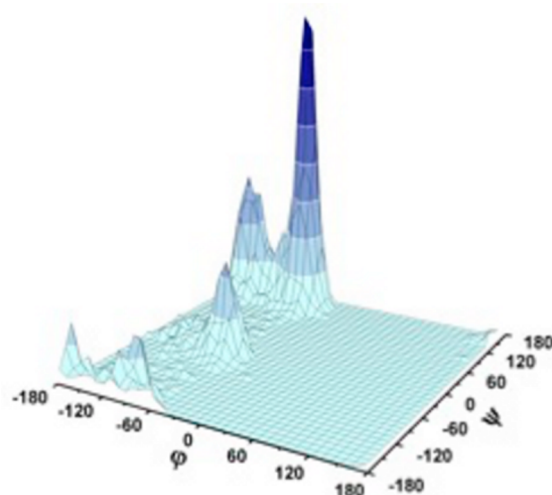


Figure 7. GANHMe (ϕ , ψ) probability distribution in water as found by MD simulations.

conformer, which has the strongest NHCO intramolecular hydrogen bond in the Gly-Ala and the C7eq-C7ax conformers, with an intramolecular hydrogen bond and a cyclic form in order to minimize the external accessible surface. In solution, the most stable conformers instead have high molecular dipole moments, and they are stabilized by solute–solvent interactions, such as in β -like (β_2 and PPII) or α -helices structures (α_R and α_L for right- and left-handed helices). More complex foldings could be possible depending on the solvent, like in α_D and α'_D forms in water where external polar groups are stabilized by specific hydrogen bonds. After full optimization of all the initial structures in water solution with the PCM continuum approach, four representative stable minima were identified. A pictorial view of the optimized structures together with the indication of the conformational ϕ and ψ angles and the relative Boltzmann populations are given in Figure 8.

If we apply the labeling scheme for peptides in solution using the β , PPII, and α_R regions, GANHMe in water is predominantly found in the PPII arrangement (two different minima are found, Conformer 1 and Conformer 3, summing up

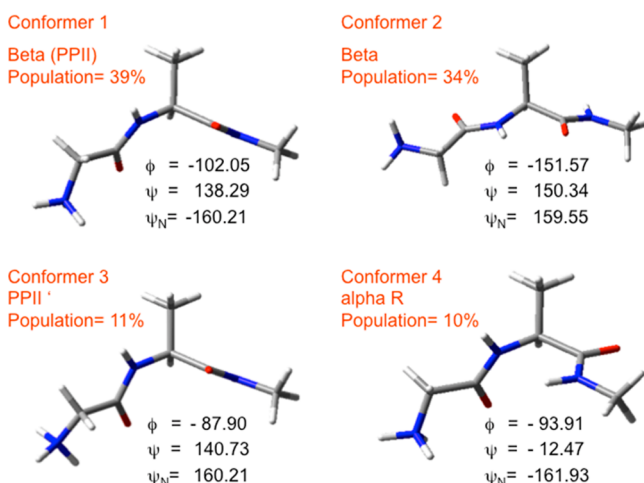


Figure 8. GANHMe most stable structures in water and relative populations calculated with PCM model.

to a total population of 50%), followed by β -strand (Conformer 2 with a population of 34%), and finally by α_R conformations (Conformer 4 with only a 10% population).

These data are consistent with experimental and theoretical findings,^{63–70} which have demonstrated that fairly well-defined structures can persist locally even in disordered peptides. Indeed, the α -helix, β -strand (and γ -turn) conformations are stabilized by a combination of local and nonlocal peptide–solvent interactions, whereas the PPII structure reflects the propensity of each single residue. Several L-Alanine-based oligopeptides^{61,71–75} occupy a mixture of PPII and β -strand conformations, and in some of these molecules, the PPII arrangement seems preferred.

In order to confirm the PCM-QM results, MD simulations have been carried out. The sampled conformations with the 5 ns unconstrained simulation at 300 K were analyzed considering backbone dihedral angles (ϕ , ψ) and the angle θ between the two CO transition dipole vectors,⁷⁶ in order to compare theoretical and experimental findings. The conformational behavior of GANHMe in terms of the (ϕ , ψ) pair is described focusing our attention on the previously recalled important regions of the Ramachandran maps, namely β , PPII, and α_R regions.^{77,78} In Figure 7, where the (ϕ , ψ) probability distribution is shown, three distinct peaks assigned to the α_R , β , and PPII conformations can be noticed. As it appears from the height of the peaks, the force field description predicts that GANHMe in water is predominantly found in the extended β and PPII conformations, having a total population of about 74%, with the dominant contribution coming from the PPII-like arrangement (42%), whereas the α_R region is less populated (18%). The population analysis that is obtained by exploiting the MD approach is in very good agreement with PCM-QM data, thus reporting the reliability of the PCM continuum model in predicting the conformational properties of GANHMe.

Comparing the results reported in Table 1 with those shown in Figure 8 we can see that once again the agreement between

Table 1. Relative MD Population Probabilities of the Major Conformations PPII, β , and α_R and Average Dihedral Angles with Their Standard Deviations

	pop (%)	ϕ		ψ		ψ_N	
		average	σ	average	σ	average	σ
PPII	42	-73	12	153	16	± 162	20
β^a	32	-144	21	156	15	± 162	20
		-144	21	-167	13		
α_R	18	-88	28	-21	22	± 162	20

^aThe two reported values correspond to two conformers found with MD simulations. Note that PPII and PPII' conformers are distinguished by PCM calculations but not by MD.

MD and PCM-QM is quite good (only for the ϕ angle of PPII, the MD average value is less negative than in the QM calculations, namely $-73 \pm 12^\circ$ with respect to -102° and -88°).

As a side note, we add a comment on the ψ_N dihedral angle. Table 1 shows that two peaks centered at $\pm 162^\circ \pm 20^\circ$ are equally sampled in all of the identified conformations. A very similar picture was found at the PCM-QM level; such a preference was clearly explained due to the attractive interactions between the charged NH_3^+ group and the closest carbonyl oxygen. By contrast, all structures with a smaller

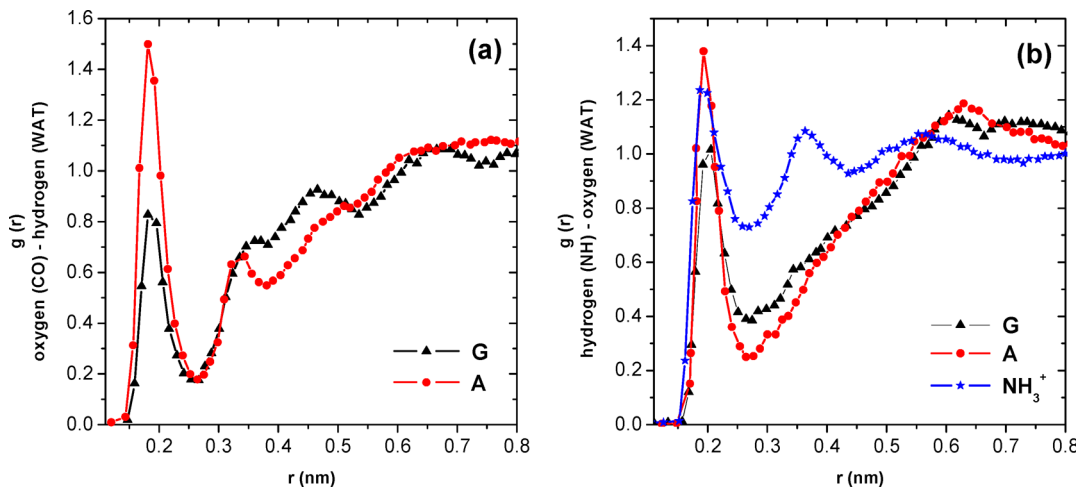


Figure 9. Atom–atom radial distribution functions of CO–H_{water} (a) and NH–O_{water} (b). G = Glycine, A = L-Alanine, NH₃⁺ = N charged terminus.

dihedral ψ_N angle led to very high-energy structures due to the repulsive interactions with the closest amide proton.

Due to the chemical nature of the GANHMe–water solvated system, it is natural to assess the presence of specific GANHMe–water hydrogen bonding interactions as seen also in linear and 2D spectra. The structures obtained by exploiting the basic PCM approach only account for the electrostatic part of the water interactions, but the specific hydrogen bond network around GANHMe, which leads to anisotropy in the solute–solvent interactions and eventually to solute–solvent charge transfer effects, cannot be properly described by the PCM. Refinements in the approach are necessary, such as the inclusion in the molecular system of some explicit solvent molecules around the solute (the so-called supermolecule approach⁴¹).

In order to better investigate the hydrogen bonding effects and pattern, Amber MD simulations were performed starting from the most stable GANHMe structure corresponding to Conformer 1, kept fixed during the simulation, but allowing the water molecules to rearrange around it.

The large number of hydrophilic sites present in the GANHMe peptide are responsible for a definite anisotropic structure of the surrounding solvent molecules, which can be described by means of radial distribution (RD) analysis: RD plots in D₂O and DMSO are shown in Figure 9 and 10, respectively.

Water is both hydrogen bond acceptor and donor to NH and CO peptide groups. This gives a clear preference for water to enter the first solvation shell as it can be noticed from the examination of the RDFs calculated between the solvent molecules and each carbonyl oxygen and amidic hydrogen of GANHMe. All of the trends suggest the presence of strong hydrogen bonds, exhibiting sharp peaks at 1.8 and 2.0 Å for oxygens and amidic hydrogens, respectively. For both amide hydrogens, there is one water molecule in the first peak assumed to be hydrogen bonded, whereas the charged terminus region (NH₃⁺) is surrounded by a greater number of water molecules which are arranged in two ordered hydration shells (2 and 9 waters in the first and second shell) represented by the two well-defined peaks centered at 2.0 and 3.5 Å, respectively. The tendency to specific ordering of water beyond the first hydration sphere is also observed in the case of L-Alanine oxygen, where two distinct shells can be clearly identified.

The coordination number obtained from the integration of the first peak of the RDF centered at about 1.8 Å is about 2, and the smaller second peak centered at about 3.1 Å gives indication of a H-bond-like arrangement of other two water molecules (four waters in all). In contrast, the integration of the first peak of the Glycine oxygen reveals the presence of a H-bond-like complex of this moiety with just one water molecule. Exchange of waters between the first and second solvation shells is observed for each GANHMe site. The average lifetime of water–GANHMe hydrogen bonds is about 1.1 ps, similar to the measured vibrational lifetime: this is consistent with the experimental observation that the spectral diffusion occurs on the same time of the vibrational relaxation. Hydrogen bonds involving GANHMe oxygen atoms have a longer average lifetime (1.5 ps) and an average percentage of occupancy of about 78%. Instead, H bonds engaging both amide hydrogens have the lowest average percentage of occupancy (about 42%); however, their average lifetime (1.1 ps) is equal to the one determined for the NH₃⁺ terminus group which, on the other hand, shows a greater average percentage of occupancy (about 64%).

From these findings, it is clear that a relatively strongly structured H-bond network is present around H(N) and O(C) of GANHMe in water. Since Amide I involves mainly the CO stretching, we shall limit the analysis of possible H-bonding effects on those acting on the carbonyl oxygens only. As recalled before, a very effective way to accurately take into account such effects is the supermolecule approach in which clusters, containing the GANHMe plus few H-bonded water molecules, are optimized at QM level including the bulk effects of the rest of the solvent using the PCM. In particular, two different clusters were constructed, starting with the most stable GANHMe conformer and adding two or four water molecules properly arranged around CO sites.

In Table 2, we report the calculated Amide I frequencies, the corresponding shifts ($\Delta\nu$), and the θ angle for the four conformers indicated in Figure 8.

Small absolute differences are found in the two frequencies as a function of GANHMe conformation, but the resulting splitting values are significantly changed passing from PPII to β and more to α_R . The splitting obtained by averaging weighted conformer Boltzmann populations is 25 cm⁻¹, comparable with the experimental value of 28 cm⁻¹.

Table 2. PCM-QM Calculated Amide I Frequencies ν_1 -Ala and ν_2 -Gly (cm^{-1}) and Angle θ (deg) between Transition Dipole Vectors of Relevant GANHMe Conformers in Water

	pop (%)	ν_1	ν_2	$\Delta\nu$	θ
exp		1646.3	1674.7	28	60
PPII	40	1682	1704	22	49
β	34	1675	1702	27	63
PPII'	10	1684	1705	21	53
α_R	10	1674	1709	35	106
average				25	61

Another way to obtain an average splitting is that of using MD populations (see Table 1), instead of the PCM-QM ones. In doing that, the average splitting becomes 27 cm^{-1} .

To check further, we have repeated the vibrational calculations for the two clusters with two and four explicit water molecules. Calculated vibrational frequencies of the Amide I modes of clusters generally decrease with respect to the corresponding values for GANHMe, going toward the experimental findings but not in the same way for the two modes. As a result, the splitting increases 5 and 24% with two and four water molecules, respectively. This analysis, even if limited to a single conformer, seems to show that H-bond effects on the carbonyl groups induce a larger splitting, thus leading toward a more quantitative agreement with experiments.

A final analysis of the results reported in Table 2 is on the angle θ between the transition dipole vectors. Such values are by far more sensitive to GANHMe conformation than the corresponding frequencies and range from 49 (PPII) to 106 deg (α_R). On average, the value of 61 deg is obtained. Note that the angle values are obtained by considering the Cartesian coordinates of the calculated transition dipole vectors, without resorting to any other assumption.

The θ angle can also be estimated from MD using only structural information and assuming that the transition dipole moments can be represented as vectors forming an angle of 20 deg with respect to the vector aligned along the C=O group².

The values for PPII, β , and α_R conformations are 73, 63, and 104 degrees, respectively. These values are in very good agreement with the QM values reported in Table 2, which

show, once more, the parallel description obtained with the two approaches.

3.2.2. Conformational Study of GANHMe in DMSO. In order to compare the differences due to the interaction of GANHMe with a protic or an aprotic solvent, we decided to carry out MD simulations of GANHMe in DMSO using the same geometry investigated in water (Conformer 1). This was kept fixed during the whole simulation time, whereas DMSO molecules were allowed to rearrange around it. Figure 10 represents the radial orientations of hydrogen and oxygen atoms of DMSO around the molecule.

Because DMSO a hydrogen bond acceptor, it is preferentially located around the NH groups of GANHMe. The first coordination shell of GANHMe carbonyl oxygens is represented by two broad and low peaks centered at about 2.63 Å (with a minimum at about 3.62 Å) with coordination numbers of 5.0 and 6.2 for Gly and Ala oxygens, respectively. These data indicate that both GANHMe oxygens are engaged in weak interactions with the nearby DMSO molecules, which orient their methyl hydrogens toward the peptide oxygen sites thus forming $-\text{CH}\cdots\text{O}$ pairs. Smaller second peaks centered at about 4.2 Å with a minimum at about 4.8 Å are also visible, suggesting that methyl hydrogens form an organized shell beyond the first solvation sphere around the GANHMe peptide oxygens. As far as the amide hydrogens are concerned, a single sharp peak with a maximum at about 1.9 Å and coordination number equal to 1.0 is observed, suggesting that only one DMSO molecule is hydrogen bonded to these groups and solvent molecules are not ordered beyond this first solvation shell, whereas NH_3^+ RD function shows two distinct peaks, a well-defined peak centered at about 2.0 Å with coordination number equal to 1.9 and a smaller and broader one with a maximum at a rather large separation of 3.4 Å. This finding suggests a specific ordering of DMSO molecules in the second solvation sphere. However, for this moiety, solvent organization seems to extend also beyond the second shell as confirmed by the presence of a very broad third peak, hardly discernible, centered at about 5.8 Å. Even though the average percentage of occupancy of hydrogen bonds between the GANHMe sites and DMSO molecules (3%) is lower than the one observed in the case of water (62%), their average lifetime is longer, calculated as about 2.1 ps (maximum average lifetime = 2.6 ps).

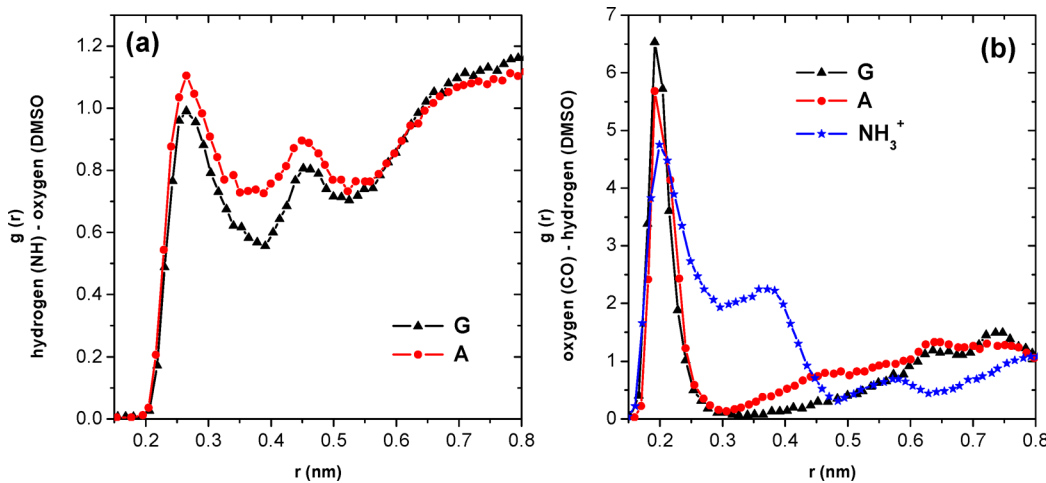


Figure 10. Atom-atom radial distribution functions for GANHMe in DMSO. G = Glycine, A = L-Alanine, NH_3^+ = N charged terminus.

The differences between solvents are most likely due to the different orientation and the lower coordination number of DMSO molecules due to steric hindrance.

From the examination of the RD functions, it is clear that DMSO acts primarily as a hydrogen bond acceptor and solvates predominantly the regions close to the NH groups. Indeed, the positions of its hydrogen atoms are greatly separated (about 2.6 Å) and cannot be viewed as an indication of a strong H-bond donor. On the contrary, water molecules around the GANHMe oxygen atoms form two pronounced solvation shells characterized by high density levels. From the MD findings, it comes out that the GANHMe carbonyl groups interact with the methyl hydrogens of DMSO. This should cause a decrease in the solute–solvent mutual polarization with respect to water because the interaction between the polar carbonyl groups of GANHMe and polar SO groups of DMSO is in some way screened by the presence of the methyl groups. In order to model such a reduced interaction with PCM, a different choice in the molecular cavity surrounding the solute was completed. In particular, since DMSO is distributed around GANHMe so that larger distances are found between GANHMe and DMSO carbonyl groups (with respect to the GANHMe–water system), it seems reasonable to exploit a larger cavity scale factor for the carbonyl oxygens, namely, 1.4 instead of the default value of 1.2 nm.

Using such a modified cavity, the initial 10 structures used to get conformers in water were reoptimized in DMSO. As for water, four conformers were found; the corresponding populations and vibrational properties are reported in Table 3.

Table 3. PCM-QM Calculated Amide I Frequencies ν_1 -Ala and ν_2 -Gly (cm^{-1}) and Angle θ (deg) between Transition Dipole Vectors of Relevant GANHMe Conformers in DMSO

	pop (%)	ν_1	ν_2	$\Delta\nu$	θ
exp		1671	1689	18	40
β	40	1690	1714	24	65
PPII	31	1701	1716	15	58
PPII'	25	1701	1720	19	36
α_R	4	1691	1720	29	109
average				20	57

By comparing the populations reported in Table 3 with those reported in Table 2 for water, a substantial decrease in the population of the α_R structure is observed along with a less pronounced decrease of the weight of PPII and a parallel increase in the population of the β structure. The tendency of small peptides to maintain the conformation of the single residue is reinforced in the aprotic solvents.

A further validation of the conformation analysis is done on the coupling constants. The experimental values of the coupling constant obtained from linear spectra are $10 \pm 2 \text{ cm}^{-1}$ in D_2O and $7 \pm 3 \text{ cm}^{-1}$ in DMSO and from 2D spectra are $15 \pm 4 \text{ cm}^{-1}$ in D_2O and $10 \pm 5 \text{ cm}^{-1}$ in DMSO (see Supporting Information). By following the Hessian matrix reconstruction method,^{79–81} values of 6 cm^{-1} for DMSO and of 7 cm^{-1} for D_2O are obtained by averaging over the four main conformations. In the model, the normal mode is calculated as a combination of a limited number of specific local modes, and the geometrical deviation from the exact normal mode is minimized. We observe that we are able to reproduce the order of magnitude, but it is difficult to appreciate differences between the molecule in the two solvents. The Hessian matrix

reconstruction provides an estimate of the global coupling deriving from both through-bond and through-space interactions. By evaluating the transition dipole moments from calculated geometries, it is possible to estimate the dipole–dipole interaction. This results to be around 2 cm^{-1} in both solvents. This confirms the prevalence of the through-bond coupling.

4. CONCLUSIONS

Two-dimensional spectral data provide evidence that in short peptides in solution and at room temperature there is a distribution of conformations. We demonstrate that by combining 2D-IR measurements and a conformational analysis, including the solvent on GANHMe, it is possible to determine the prevalent structures as a function of the solvent nature. By comparing the calculated molecular properties, averaged over the conformer population, experimental values are reproduced in quite good agreement. We clarify the role of solvents in determining the static and dynamic properties of the system. In short peptides there is a prevalence of β -like structures dominated by the single residue behavior.

The evolution of the 2D spectra is consistent with a spectral diffusion dominated by the solvent dynamics. In water, the fast hydrogen bond dynamics is comparable to that of the vibrational relaxation, while in DMSO it occurs on a time scale twice longer.

The population decay of the Amide I modes has been measured and resulted to be $1.2 \pm 0.2 \text{ ps}$ in both solvents. This result is consistent with previous ones on different type of peptides. The intramolecular energy decay processes are dominant in the deactivation of the Amide I mode.

A final observation is that the coupling between Amide I modes is small, and it is essentially driven by the through-bond mechanism.

■ ASSOCIATED CONTENT

S Supporting Information

Detailed calculations of the coupling constants from both linear IR and 2D-IR spectra are reported. This information is available free of charge via the Internet at <http://pubs.acs.org>

■ AUTHOR INFORMATION

Corresponding Author

*E-mail: foggi@lens.unifi.it. Fax: +39 055 4572521. Tel.: +39 055 4572494.

Notes

The authors declare no competing financial interest.

■ ACKNOWLEDGMENTS

The authors wish to remember Robin M. Hochstrasser, recently deceased, who gave the largest contribution to the development of 2DIR spectroscopy. The authors acknowledge the Italian “Ministero dell’Istruzione, dell’Università e della Ricerca” (PRIN 2008BFJ34R, FIRB RBFR10Y5VW, and EFOR L. 191/2009 art. 2 comma 44) and the “Ente Cassa di Risparmio di Firenze” for their financial support. Moreover, A.M.P. thanks the ANR Chaire d’Excellence 2009-2013 for financial support to PeptLab.

■ REFERENCES

- (1) Gremlach, H. U.; Yan, B. *Infrared and Raman Spectroscopy of Biological Materials*; Marcell Dekker, Inc.: New York, 2001.

- (2) Krimm, S.; Bandekar, J. Vibrational Spectroscopy and Conformation of Peptides, Polypeptides and Proteins. *J. Adv. Protein Chem.* **1986**, *38*, 181–364.
- (3) Raid, G. D.; Wynne, K. *Ultrafast Laser Technology and Spectroscopy. Encyclopedia of Analytical Chemistry*; John Wiley & Sons, Ltd: Chichester, U.K., 2000; pp 13644–13670.
- (4) Fayer, M. D. Fast Protein Dynamics Probed with Infrared Vibrational Echo Experiments. *Annu. Rev. Phys. Chem.* **2001**, *52*, 315–356.
- (5) Woutersen, S.; Hamm, P. Nonlinear Two-Dimensional Vibrational Spectroscopy of Peptides. *J. Phys.: Condens. Matter* **2002**, *14*, R1035–R1062.
- (6) Tokmakoff, A. Two-Dimensional Line Shapes Derived from Coherent Third-Order Nonlinear Spectroscopy. *J. Phys. Chem. A* **2000**, *104*, 4247–4255.
- (7) Hamm, P.; Zanni, M. *Concepts and Methods of 2D Infrared Spectroscopy*; Cambridge University Press: Cambridge, 2011.
- (8) Mukamel, S. *Principles of Nonlinear Optical Spectroscopy*; Oxford University Press: New York, 1995.
- (9) Cho, M. *Two-Dimensional Optical Spectroscopy*; CRC Press: New York, 2009.
- (10) Woutersen, S.; Hamm, P. Isotope-Edited Two-Dimensional Vibrational Spectroscopy of TriAlanine in Aqueous Solution. *J. Chem. Phys.* **2001**, *114*, 2727–2737.
- (11) Asplund, M. C.; Zanni, M. T.; Hochstrasser, R. M. Two-Dimensional Infrared Spectroscopy of Peptides by Phase-Controlled Femtosecond Vibrational Photon Echoes. *Proc. Natl. Acad. Sci. U.S.A.* **2000**, *97*, 8219–8224.
- (12) Kim, S. Y.; Hochstrasser, R. M. Chemical Exchange 2D-IR of Hydrogen-Bond Making and Breaking. *Proc. Natl. Acad. Sci. U.S.A.* **2005**, *102*, 11185–11190.
- (13) Hamm, P.; Lim, M.; Hochstrasser, R. M. Structure of the Amide I Band of Peptides Measured by Femtosecond Nonlinear-Infrared Spectroscopy. *J. Phys. Chem. B* **1998**, *102*, 6123–6138.
- (14) Lima, M.; Candelaresi, M.; Foggi, P. 2D-IR Spectroscopy: An Additional Dimension to Investigate Ultrafast Structural Dynamics. *J. Raman Spectrosc.* **2013**, *44*, 1470–1477.
- (15) Scheurer, C.; Mukamel, S. Magnetic Resonance Analogies in Multidimensional Vibrational Spectroscopy. *Bull. Chem. Soc. Jpn.* **2002**, *75*, 989–999.
- (16) Scheurer, C.; Mukamel, S. Design Strategies for Pulse Sequences in Multidimensional Optical Spectroscopies. *J. Chem. Phys.* **2001**, *115*, 4989–5004.
- (17) Torii, H.; Tasumi, M. Ab Initio Molecular Orbital Study of the Amide I Vibrational Interactions Between the Peptide Groups in Di- and Tri-Peptides and Considerations on the Conformation of the Extended Helix. *J. Raman Spectrosc.* **1998**, *29*, 81–86.
- (18) Zanni, M.; Hochstrasser, R. M. Two-Dimensional Infrared Spectroscopy (2DIR): A Promising New Method for the Time Resolution of Structures. *Curr. Opin. Struct. Biol.* **2001**, *11*, 516–522.
- (19) Krummel, A. T.; Mukherjee, P.; Zanni, M. T. Inter and Intrastrand Vibrational Coupling in DNA Studied with Heterodynied 2D-IR Spectroscopy. *J. Phys. Chem. B* **2003**, *107*, 9165–9169.
- (20) Moran, S. D.; Woys, A. M.; Buchanan, L. E.; Bixby, E.; Decatur, S. M.; Zanni, M. T. Two-Dimensional IR Spectroscopy and Segmental ¹³C Labeling Reveals the Domain Structure of Human Amyloid Fibrils. *Proc. Natl. Acad. Sci. U.S.A.* **2012**, *109*, 3329–3334.
- (21) Woutersen, S.; Hamm, P. Subpicosecond Conformational Dynamics of Small Peptides Probed by Two-Dimensional Vibrational Spectroscopy. *Proc. Natl. Acad. Sci. U.S.A.* **2001**, *98*, 11254–11258.
- (22) Kim, Y. S.; Hochstrasser, R. M. Two-Dimensional Infrared Spectroscopy of the Alanine Dipeptide in Aqueous Solution. *J. Chem. Phys. B* **2005**, *109*, 7511–7521.
- (23) Piryatinski, A.; Tretiak, S.; Chernyak, V.; Mukamel, S. Simulations of Two-Dimensional Femtosecond Infrared Photon Echoes of Glycine Dipeptide. *J. Raman Spectrosc.* **2000**, *31*, 125–135.
- (24) Woutersen, S.; Hamm, P. Structure Determination of TriAlanine in Water Using Polarization Sensitive Two-Dimensional Vibrational Spectroscopy. *J. Phys. Chem. B* **2000**, *104*, 11316–11320.
- (25) Zhuang, W.; Ambravicius, D.; Mukamel, S. Dissecting Coherent Vibrational Spectra of Small Proteins into Secondary Structural Elements by Sensitivity Analysis. *Proc. Natl. Acad. Sci. U.S.A.* **2005**, *102*, 7443–7448.
- (26) Hochstrasser, M. R.; Ge, N. H.; Gnanakaran, S.; Zanni, M. T. Two-Dimensional Infrared Spectroscopy: Studies of the Dynamics of Structures with Femtosecond Pulse Fourier Transform Correlation Spectroscopy. *Bull. Chem. Soc. Jpn.* **2002**, *75*, 1103–1110.
- (27) Candelaresi, M.; Foggi, P.; Lima, M.; Palmer, J. D.; Mennucci, B.; Cappelli, C.; Monti, S. Two-Dimensional Infrared Spectroscopy of Glycine-L-Alanine-Methylamide. *Ultrafast Phenomena XVI. Proc. 16th Int. Conf., Springer Series in Chemical Physics* **2010**, *92*, 418–420.
- (28) Volkov, V. V.; Palmer, D. J.; Righini, R. Heterogeneity of Water at the Phospholipid Membrane Interface. *J. Phys. Chem. B* **2007**, *111*, 1377–1383.
- (29) Woutersen, S.; Hamm, P. Time-Resolved Two-Dimensional Vibrational Spectroscopy of a Short α -Helix in Water. *J. Chem. Phys.* **2001**, *115*, 7737–7743.
- (30) Cheatum, C. M.; Tokmakoff, A. Signatures of β -Sheet Secondary Structures in Linear and Two-Dimensional Infrared Spectroscopy. *J. Chem. Phys.* **2004**, *120*, 8201–8214.
- (31) Kiso, Y.; Matsumoto, H.; Mizumoto, S.; Kimura, T.; Fujiwara, Y.; Akaji, K. Small Dipeptide-Based HIV Protease Inhibitors Containing the Hydroxymethylcarbonyl Isostere as an Ideal Transition-State Mimic. *Biopolymers* **1999**, *51*, 59–68.
- (32) Goodman, M.; Zhu, Q.; Kent, D. R.; Amino, Y.; Iacovino, R.; Benedetti, E.; Santini, A. A. Conformational Analysis of the Dipeptide Taste Ligand L-Aspartyl-d-2-aminobutyric Acid-(S)- α -Ethylbenzylamide and its Analogues by NMR Spectroscopy, Computer Simulations and X-ray Diffraction Studies. *J. Pept. Sci.* **1997**, *3*, 231–241.
- (33) Simone, G. D.; Lombardi, A.; Galdiero, S.; Nastri, F.; Costanzo, L. D.; Sano, A.; Yamada, T.; Pavone, V. The Crystal Structure of a Dcp-Containing Peptide. *Biopolymers* **2000**, *53*, 182–188.
- (34) Torreggiani, A.; Tampa, M.; Fini, G. Binding of Copper(II) to Carnosine: Raman and IR Spectroscopic Study. *Biopolymers* **2000**, *57*, 149–159.
- (35) Shendage, D. M.; Fröhlich, R.; Haufe, G. Highly Efficient Stereoconservative Amidation and Deamidation of α -Amino Acids. *Org. Lett.* **2004**, *6*, 3675–3678.
- (36) Engelfried, C.; Ludwig, K.; Jaenichen, H.; Koenig, W. A. Reaktionen von Aminosäuren und Peptiden, II. Darstellung von 2-Aminooxazolderivaten aus Peptidamiden mit Hexafluoracetanhydrid. *Liebigs Annalen der Chemie* **1979**, *7*, 973–985.
- (37) Hamm, P.; Kaindl, R. A.; Stenger, J. Noise Suppression in Femtosecond Mid-Infrared Light Sources. *Opt. Lett.* **2000**, *25*, 1798–1800.
- (38) Prevedelli, M. *Double Linear Array MCT Front-End. LENS*, 2003. <http://lens.unifi.it/ew/>
- (39) Cancès, E.; Mennucci, B.; Tomasi, J. A New Integral Equation Formalism for the Polarizable Continuum Model: Theoretical Background and Applications to Isotropic and Anisotropic dielectrics. *J. Chem. Phys.* **1997**, *107*, 3032–3041.
- (40) Mennucci, B.; Cancès, E.; Tomasi, J. Evaluation of Solvent Effects in Isotropic and Anisotropic Dielectrics and in Ionic Solutions with a Unified Integral Equation Method: Theoretical Bases, Computational Implementation, and Numerical Applications. *J. Phys. Chem. B* **1997**, *101*, 10506–10517.
- (41) Tomasi, J.; Mennucci, B.; Cammi, R. Quantum Mechanical Continuum Solvation Models. *Chem. Rev.* **2005**, *105*, 2999–3093.
- (42) Frisch, M. J.; Trucks, G. W.; Schlegel, H. B.; Scuseria, G. E.; Robb, M. A.; Cheeseman, J. R.; Montgomery, J. A., Jr.; Vreven, T.; Kudin, K. N.; Burant, J. C.; Millam, J. M.; Iyengar, S. S.; Tomasi, J.; Barone, V.; Mennucci, B.; Cossi, M.; Scalmani, G.; Rega, N.; Petersson, G. A.; Nakatsuji, H.; Hada, M.; Ehara, M.; Toyota, K.; Fukuda, R.; Hasegawa, J.; Ishida, M.; Nakajima, T.; Honda, Y.; Kitao, O.; Nakai, H.; Klene, M.; Li, X.; Knox, J. E.; Hratchian, H. P.; Cross, J. B.; Bakken, V.; Adamo, C.; Jaramillo, J.; Gomperts, R.; Stratmann, R. E.; Yazayev, O.; Austin, A. J.; Cammi, R.; Pomelli, C.; Ochterski, J. W.; Ayala, P. Y.; Morokuma, K.; Voth, G. A.; Salvador, P.; Dannenberg, J.

- J.; Zakrzewski, V. G.; Dapprich, S.; Daniels, A. D.; Strain, M. C.; Farkas, O.; Malick, D. K.; Rabuck, A. D.; Raghavachari, K.; Foresman, J. B.; Ortiz, J. V.; Cui, Q.; Baboul, A. G.; Clifford, S.; Cioslowski, J.; Stefanov, B. B.; Liu, G.; Liashenko, A.; Piskorz, P.; Komaromi, I.; Martin, R. L.; Fox, D. J.; Keith, T.; Al-Laham, M. A.; Peng, C. Y.; Nanayakkara, A.; Challacombe, M.; Gill, P. M. W.; Johnson, B.; Chen, W.; Wong, M. W.; Gonzalez, C.; Pople, J. A. *Gaussian 03*, revision C.02; Gaussian, Inc.: Wallingford, CT, 2004.
- (43) Mennucci, B.; Martinez, J. How to Model Solvation of Peptides? Insights from a Quantum-Mechanical and Molecular Dynamics Study of N-Methylacetamide. 1. Geometries, Infrared, and Ultraviolet Spectra in Water. *J. Phys. Chem. B* **2005**, *109*, 9818–9829.
- (44) Mennucci, B.; Martinez, J. How to Model Solvation of Peptides? Insights from a Quantum Mechanical and Molecular Dynamics Study of N-Methylacetamide. 2. ^{15}N and ^{17}O Nuclear Shielding in Water and in Acetone. *J. Phys. Chem. B* **2005**, *109*, 9830–9838.
- (45) Cappelli, C.; Mennucci, B. Modeling the Solvation of Peptides. The Case of (s)-N-Acetylproline Amide in Liquid Water. *J. Phys. Chem. B* **2008**, *112*, 3441–3540.
- (46) Cappelli, C.; Monti, S.; Scalmani, G.; Barone, V. On the Calculation of Vibrational Frequencies for Molecules in Solution Beyond the Harmonic Approximation. *J. Chem. Theory Comput.* **2010**, *6*, 1660–1669.
- (47) Biancardi, A.; Cappelli, C.; Mennucci, B.; Cammi, R. Toward a Quantum-Mechanical Description of 2D-IR Spectra of Solvated Systems: The Vibrational Mode Coupling within A Polarizable Continuum Model. *J. Phys. Chem. B* **2010**, *114*, 4924–4930.
- (48) Case, D. A. et al. AMBER 9; University of California, San Francisco, 2006.
- (49) Duan, Y.; Wu, C.; Chowdhury, S.; Lee, M. C.; Xiong, G.; Zhang, W.; Yang, R.; Cieplak, P.; Luo, R.; Lee, T.; Caldwell, J.; Wang, J.; Kolmann, P. A. A Point-Charge Force Field for Molecular Mechanics Simulations of Proteins Based on Condensed-Phase Quantum Mechanical Calculations. *J. Comput. Chem.* **2003**, *24*, 1999–2012.
- (50) Lee, M. C.; Duan, Y. Distinguish Protein Decoys by Using a Scoring Function Based on a New AMBER Force Field, Short Molecular Dynamics Simulations, and the Generalized Born Solvent Model. *Proteins* **2004**, *55*, 620–634.
- (51) Wang, J.; Cieplak, P.; Kollman, P. A. How Well Does a Restrained Electrostatic Potential (RESP) Model Perform in Calculating Conformational Energies of Organic and Biological Molecules. *J. Comput. Chem.* **2000**, *21*, 1049–1074.
- (52) Mu, Y.; Kosov, D. S.; Stock, G. Conformational Dynamics of Trialanine in Water. Comparison of AMBER, CHARMM, GROMOS, and OPLS Force Fields to NMR and Infrared Experiments. *J. Phys. Chem. B* **2003**, *107*, 5064–5073.
- (53) Jorgensen, W. L. Quantum and Statistical Mechanical Studies of Liquids. Transferable Intermolecular Potential Functions for Water, Alcohols and Ethers. Application to Liquid Water. *J. Am. Chem. Soc.* **1981**, *103*, 335–350.
- (54) Fox, T.; Kollman, P. A. Application of the RESP Methodology in the Parametrization of Organic Solvents. *J. Phys. Chem. B* **1998**, *102*, 8070–8079.
- (55) Berendsen, H. J. C.; Postma, J. P. M.; Van Gunsteren, W. F.; Di Nola, A.; Haak, J. R. Molecular Dynamics With Coupling to an External Bath. *J. Chem. Phys.* **1984**, *81*, 3684–3690.
- (56) Andrea, T. A.; Swope, W. C.; Andersen, H. C. The Role of Long Ranged Forces in Determining the Structure and Properties of Liquid Water. *J. Chem. Phys.* **1983**, *79*, 4576–4584.
- (57) Andersen, H. C. Molecular Dynamics Simulations at Constant Pressure and/or Temperature. *J. Chem. Phys.* **1980**, *72*, 2384–2393.
- (58) Lee, O.; Roberts, M.; Diem, M. IR Vibrational CD in Alanyl Tripeptide: Indication of a Stable Solution Conformer. *Biopolymers* **1989**, *28*, 1759–1770.
- (59) Sieler, G.; Schweitzer-Stenner, R.; Holtz, J. S. W.; Pajcini, V.; Asher, S. A. Different Conformers and Protonation States of Dipeptides Probed by Polarized Raman, UV-Resonance Raman and FTIR Spectroscopy. *J. Phys. Chem. B* **1999**, *103*, 372–384.
- (60) Hamm, P.; Lim, M.; DeGrado, F.; Hochstrasser, R. M. The Two-Dimensional IR Nonlinear Spectroscopy of a Cyclic Penta-Peptide in Relation to its Three-Dimensional Structure. *Proc. Natl. Acad. Sci. U.S.A.* **1999**, *96*, 2036–2041.
- (61) Gutierrez, L. J.; Baldoni, H. A.; Enriz, R. D. Conformational and Electronic Study of Cis-Peptides (Non-Proline Residues) Occurring in Natural Proteins. *J. Mol. Struct.* **2009**, *934*, 103–111.
- (62) Wang, Z. X.; Duan, Y. Solvation Effects on Alanine Dipeptide: A MP2/cc-pVTZ//MP2/6-31G** Study of (Φ , Ψ) Energy Maps and Conformers in the Gas Phase, Ether and Water. *J. Comput. Chem.* **2004**, *25*, 1699–1716.
- (63) Eker, F.; Greibenow, K.; Cao, X.; Nafie, L. A.; Schweitzer-Stenner, R. Preferred Peptide Backbone Conformations in the Unfolded State Revealed by the Structure Analysis of Alanine-Based (AXA) Tripeptides in Aqueous Solution. *Proc. Natl. Acad. Sci. U.S.A.* **2004**, *101*, 10054–10059.
- (64) Bochicchio, B.; Tamburro, A. M. Polyproline II Structure in Proteins: Identification by Chiroptical Spectroscopies, Stability and Functions. *Chirality* **2002**, *14*, 782–792.
- (65) Shi, Z.; Woody, R. W.; Kallenbach, N. R. Is Polyproline II a Major Backbone Conformation in Unfolded Proteins? *Adv. Protein Chem.* **2002**, *62*, 163–240.
- (66) Dill, K. A. Polymer Principles and Protein Folding. *Protein Sci.* **2002**, *8*, 1166–1180.
- (67) Han, W. G.; Jalkanen, J.; Elstner, M.; Suhai, S. Theoretical Study of Aqueous N-Acetyl-L-Alanine N'-Methylamide: Structures and Raman, VCD, and ROA Spectra. *J. Phys. Chem. B* **1998**, *102*, 2587–2602.
- (68) Weise, C. F.; Weisshaar, J. C. Conformational Analysis of Alanine Dipeptide from Dipolar Couplings in a Water-Based Liquid Crystal. *J. Phys. Chem. B* **2003**, *107*, 3265–3277.
- (69) Eker, F.; Cao, X.; Nafie, L. A.; Huang, Q.; Schweitzer-Stenner, R. The Structure of Alanine Based Tripeptides in Water and Dimethyl Sulfoxide Probed by Vibrational Spectroscopy. *J. Phys. Chem. B* **2003**, *107*, 358–365.
- (70) Pappu, R. V.; Rose, G. D. A Simple Model for Polyproline II Structure in Unfolded States of Alanine-Based Peptides. *Protein Sci.* **2002**, *11*, 2437–2455.
- (71) Park, S. H.; Shalongo, W.; Stellwagen, E. The Role of PII Conformations in the Calculation of Peptide Fractional Helix Content. *Protein Sci.* **1997**, *6*, 1694–1700.
- (72) Olson, Z. S. C. A.; Rose, G. D.; Baldwin, R. L.; Kallenbach, N. R. Polyproline II Structure in a Sequence of Seven Alanine Residues. *Proc. Natl. Acad. Sci. U.S.A.* **2002**, *99*, 9190–9195.
- (73) Eker, F.; Cao, X.; Nafie, L. A.; Schweitzer-Stenner, R. Tripeptides Adopt Stable Structures in Water. A Combined Polarized Visible Raman, FTIR, and VCD Spectroscopy Study. *J. Am. Chem. Soc.* **2002**, *124*, 14330–14341.
- (74) Toal, S.; Meral, D.; Verbaro, D.; Urbanc, B.; Schweitzer-Stenner, R. pH-Independence of Trialanine and the Effects of Termini Blocking in Short Peptides: A Combined Vibrational, NMR, UVCD, and Molecular Dynamics Study. *J. Phys. Chem. B* **2013**, *117*, 3689–3706.
- (75) Mu, Y.; Kosov, D. S.; Stock, G. Conformational Dynamics of Trialanine in Water. 2. Comparison of AMBER, CHARMM, GROMOS, and OPLS Force Fields to NMR and Infrared Experiments. *J. Phys. Chem. B* **2003**, *107*, 5064–5073.
- (76) Gbabakaran, S.; Hochstrasser, R. M. Conformational Preferences and Vibrational Frequency Distributions of Short Peptides in Relation to Multidimensional Infrared Spectroscopy. *J. Am. Chem. Soc.* **2001**, *123*, 12886–12898.
- (77) Brooks, C. L., III; Case, D. A. Simulations of Peptide Conformational Dynamics and Thermodynamics. *Chem. Rev.* **1993**, *93*, 2487–2502.
- (78) Head-Gordon, T.; Head-Gordon, M.; Frisch, M. J.; Brooks, C. L., III; Pople, J. A. Theoretical Study of Blocked Glycine and Alanine Peptide Analogs. *J. Am. Chem. Soc.* **1991**, *113*, 5989–5997.
- (79) Ham, S.; Cha, S.; Choi, J. H.; Cho, M.; Amide, I. Modes of Tripeptides: Hessian Matrix Reconstruction and Isotope Effects. *J. Chem. Phys.* **2003**, *119*, 1451–1461.

(80) Ham, S.; Cho, M.; Amide, I. Modes in the N-Methylacetamide Dimer and Glycine Dipeptide Analog: Diagonal Force Constants. *J. Chem. Phys.* **2003**, *118*, 6915–6922.

(81) Gorbunov, R. D.; Kosov, D. S.; Stock, G. Ab Initio-Based Exciton Model of Amide I Vibrations in Peptides: Definition, Conformational Dependence and Transferability. *J. Chem. Phys.* **2005**, *122*, 224904–225113.